

# Robust dynamical decoupling with concatenated continuous driving

J. Cai,<sup>1</sup> B. Naydenov,<sup>2</sup> R. Pfeiffer,<sup>2</sup> L. P. McGuinness,<sup>2</sup> K. D. Jahnke,<sup>2</sup> F. Jelezko,<sup>2</sup> M. B. Plenio,<sup>1</sup> and A. Retzker<sup>1,3</sup>

<sup>1</sup>*Institut für Theoretische Physik, Albert-Einstein Allee 11, Universität Ulm, 89069 Ulm, Germany*

<sup>2</sup>*Institut für Quantenoptik, Albert-Einstein Allee 11, Universität Ulm, 89069 Ulm, Germany*

<sup>3</sup>*Racah Institute of Physics, The Hebrew University of Jerusalem, Jerusalem 91904, Israel*  
(Dated: May 9, 2012)

The loss of coherence is one of the main obstacles for the implementation of quantum information processing. The efficiency of dynamical decoupling schemes, which have been introduced to address this problem, is limited itself by the fluctuations in the driving fields which will themselves introduce noise. We address this challenge by introducing the concept of concatenated continuous dynamical decoupling, which can overcome not only external noise but also fluctuations in driving fields that implement the decoupling sequences and thus holds the potential for achieving relaxation limited coherence times. We implement the scheme experimentally with nitrogen-vacancy (NV) centers in diamond, and demonstrate an improvement of the coherence time by an order of magnitude. The proposed scheme can be applied to a wide variety of other physical systems including, trapped atoms and ions, quantum dots, and may be combined with other quantum technologies challenges such as quantum sensing and quantum information processing.

*Introduction.*— Coherent control of quantum systems has opened a promising route towards novel quantum devices for quantum technologies, such as quantum information processing, quantum metrology and quantum sensing [1–4]. The performance of such quantum devices critically depends on coherence times of their constituent quantum systems which, in turn, is limited by uncontrolled interactions with their surrounding environment. This results in a challenging but fundamentally important task in current quantum experiments, namely how to protect individual quantum states from decoherence by their environment while retaining the ability to control the quantum dynamics of the system, in particular in solid state systems with characteristic complex environments. Dynamical decoupling originated in liquid state NMR and allows for the resolution of complex spectra [5]. Significant progress has been made with the theoretical proposals of various dynamical decoupling [6–13], and their experimental demonstrations [14–23].

The recently developed dynamical decoupling schemes that require only continuous oscillatory driving fields [7, 8], inherit the advantages of standard dynamical decoupling, namely requiring no encoding overhead, no quantum measurements, and no feedback controls. Moreover, they are easier to realize experimentally and are more naturally combined with other quantum information tasks, such as the implementation of high fidelity quantum gates [11–14]. In principle, one can apply continuous driving to reduce the noise suffered by a qubit considerably simply by increasing their intensity. Random and systematic fluctuations which are inevitably present in the driving field itself will ultimately limit the efficiency of dynamical decoupling. The deleterious effect of driving field fluctuations in particular will become significant when employing strong driving fields to achieve ultralong coherence times. Overcoming the limitations imposed by driving field fluctuations and thus extending

coherence times further represents a key step towards the construction of quantum memory [24], highly sensitive nano-scale magnetometers [1–3] and error-resistant quantum operation [13]. It will also be of particular interest for  $T_1$  limited Rabi-type magnetic resonance imaging, the resolution of which highly depends on the stability of microwave driving fields [25, 26].

In this Letter, we address this challenge by introducing the scheme of concatenated continuous decoupling (CCD), which can significantly extend coherence times by protecting against driving field fluctuations. As a proof-of-principle, we implement a second-order CCD with a single NV center in diamond where a second, weaker driving field, reduces the impact of the amplitude fluctuations of the first order field. We demonstrate experimentally that CCD schemes with only a weak second driving field can already increase coherence times by an order of magnitude as compared to standard schemes based on a single drive.

*Concatenated continuous dynamical decoupling* — We start by considering a two-level quantum system with the eigenstates  $|\uparrow\rangle, |\downarrow\rangle$ , see Fig.1(a). Its system Hamiltonian is  $H_0 = \frac{\hbar\omega}{2} (|\uparrow\rangle\langle\uparrow| - |\downarrow\rangle\langle\downarrow|)$ . Environmental noise causes fluctuations to the energies  $\omega_\uparrow, \omega_\downarrow$  and thus the loss of coherence. To counter such effects, we can apply a driving field on resonance with the energy gap  $\hbar\omega$  between  $|\uparrow\rangle$  and  $|\downarrow\rangle$  as

$$H_{d_1} = \hbar\Omega_1 \cos(\omega t)\sigma_x \quad (1)$$

where  $\sigma_x = |\uparrow\rangle\langle\downarrow| + |\downarrow\rangle\langle\uparrow|$ . In the interaction picture with respect to  $H_0$  and with rotating wave approximation, we find  $H_I^{(1)} = \frac{\hbar\Omega_1}{2} (|+\rangle\langle+| - |-\rangle\langle-|)$ , where  $|\pm\rangle = \frac{1}{\sqrt{2}}(|\uparrow\rangle \pm |\downarrow\rangle)$  are the dressed states. In this basis, the effect of dephasing noise now induces transitions among these dressed states, which are suppressed by an energy penalty as long as the noise power spectrum at the resonance frequency is negligible [14]. The decoupling ef-

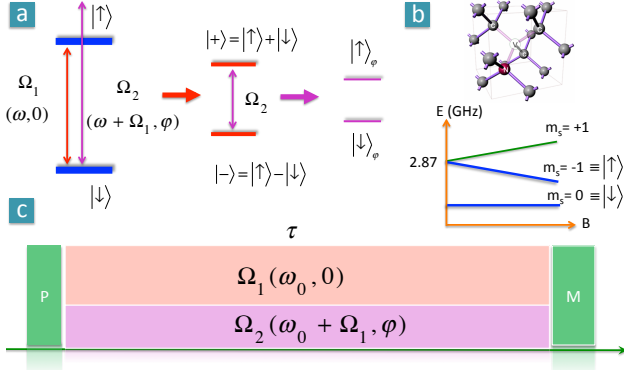


FIG. 1. (Color online) **a**: Second-order concatenated continuous dynamical decoupling: The first-order driving field with the frequency  $\omega$  and the amplitude  $\Omega_1$  creates the first-order dressed states  $|+\rangle$ ,  $|-\rangle$ , which suffer less from the dephasing effect of environment noise, however are subject to the fluctuation in the amplitude  $\Omega_1$  of the driving field. The subsequent second-order driving field with the amplitude  $\Omega_2$  (which is generally smaller than  $\Omega_1$ ) is off-resonant with the detuning  $\Omega_1$  and a relative phase  $\phi$  with respect to the first-order driving field. With such a second-order driving field, it is possible to overcome the intensity fluctuation of the first-order driving, and leads to the second-order dressed state  $|\uparrow_\varphi\rangle$  and  $|\downarrow_\varphi\rangle$  that are subject to the much reduced energy fluctuation. **b**: The diagram for the energy levels of the NV center electron spin. The NV spin triplet electronic ground state is splitted by an applied magnetic field. The effective two-level system used in our experiment is formed by the spin sublevels  $m_s = 0$  (labeled as  $|\downarrow\rangle$ ) and  $m_s = -1$  (labeled as  $|\uparrow\rangle$ ). **c**: The procedure for the Ramsey experiment with the second-order dressed qubit: the NV electron spin is first polarized into the  $m_s = 0$  sublevel, which is a coherent superposition of  $|\uparrow_\varphi\rangle$  and  $|\downarrow_\varphi\rangle$ ; the first- and second-order driving fields are simultaneously switched on for time  $\tau$  followed by the optically readout of the population of  $m_s = 0$  via spin-dependent fluorescence.

efficiency will be limited if the noise has a wide range of frequencies, while it can be very efficient for slow baths e.g. in diamond [27]. The above analysis is based on the assumption that the amplitude of the driving fields is stable. In realistic experiments however, the intensity of the driving fields will fluctuate owing to limited stability of microwave sources and amplifiers (the frequency instead can be relatively much more stable), and thus cause fluctuations of the energies of the dressed states. Achievable coherence times of the dressed qubit using a single drive are thus ultimately limited by the stability of the driving fields [25], which appears as the fast decay of Rabi oscillation.

The principal idea of CCD is to provide a concatenated set of continuous driving fields with decreasing intensities (and thus smaller absolute value of fluctuation) such that each new driving field protects against the fluctuations of the driving field at the preceding level. For example, fluctuations in the amplitude of the first-order driving

can be suppressed by applying a second-order driving field as follows

$$H_{d_2} = \hbar\Omega_2 \cos[(\omega + \Omega_1)t + \varphi]\sigma_x. \quad (2)$$

This second-order driving field is on resonance with the the energy gap of the first-order dressed state, see Fig.1 (a), which actually describes rotation about the axis  $\hat{n}(\varphi, -\pi/2)$  in the interaction picture (see SI for details) and thus plays the role of decoupling the first-order dressed states from the fluctuation of  $\Omega_1$ . With these two driving fields as  $H_{d_1}$  and  $H_{d_2}$ , we find the effective Hamiltonian in the second-order interaction picture as

$$H_I^{(2)} = \frac{\hbar\Omega_2}{4} (|\uparrow_\varphi\rangle \langle\uparrow_\varphi| - |\downarrow_\varphi\rangle \langle\downarrow_\varphi|), \quad (3)$$

where the second-order dressed states are

$$|\uparrow_\varphi\rangle = \sqrt{\frac{1}{2}} \left( \sin \frac{\varphi}{2} |\uparrow\rangle + i \cos \frac{\varphi}{2} |\downarrow\rangle \right) \quad (4)$$

$$|\downarrow_\varphi\rangle = \sqrt{\frac{1}{2}} \left( \cos \frac{\varphi}{2} |\uparrow\rangle - i \sin \frac{\varphi}{2} |\downarrow\rangle \right). \quad (5)$$

Therefore, one can encode quantum information in the above second-order dressed states as in Eq.(4-5). In general, we can apply n-order continuous driving fields on the condition that two subsequent drivings describe rotations about orthogonal axes in the corresponding interaction picture. We remark that the relative phase does not need to take a specific value, once it is fixed the corresponding second-order dressed state can serve as a robust encoded qubit see SI for details.

The decoherence of such n-th order dressed qubit stems dominantly from the fluctuation of the nth-order driving field and the residual effect of the fluctuations of the preceding driving fields. As long as the orthogonality of two consecutive driving field is satisfied, the next consecutive field reduces the noise of the previous. Hence coherence times of the nth-order dressed qubit will mainly be limited by the fluctuations of the nth-order driving field. With a concatenated scheme in which subsequent driving fields have decreasing intensities, the effective dephasing will be sequentially suppressed and coherence times of the nth-order dressed qubit can be extended significantly.

*Experimental demonstration of CCD.* — We have used NV centers in diamond to demonstrate the working principle and efficiency of our concatenated continuous dynamical decoupling scheme. As a promising candidate physical system for modern quantum technologies, NV centers have been used to demonstrate basic quantum information processing protocols [28], as well as ultra-sensitive magnetometry and nano-scale imaging at room temperature [29–31]. The electronic ground state of NV center is a spin triplet with three sublevels with magnetic quantum numbers  $m_s = 0$  and  $m_s = \pm 1$ , and the zero field splitting is  $\sim 2.87$ GHz [32], see Fig.1 (b). We apply an additional magnetic field along the axis of

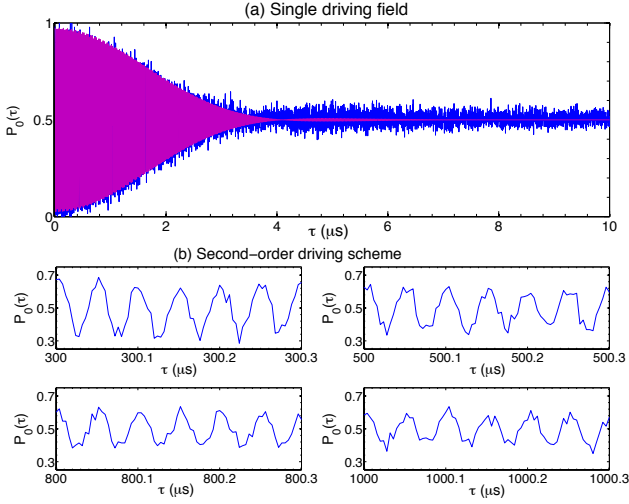


FIG. 2. (Color online) **a**: Coherent driven oscillation of NV center with a single microwave field. The Rabi frequency is  $\Omega_1 = 40\text{MHz}$ . The blue curve is the experimental data, and the purple one is the fitting with a Gaussian decay envelope. The decay time is estimated to be about  $2.5\mu\text{s}$ . **b**: Persistent Rabi oscillation by adding a second-order driving field, the intensity of which is 10 times weaker than the first driving ( $\Omega_1 = 20\text{MHz}$ ). The four panels show the very slow decay of Rabi oscillation beyond  $1000\mu\text{s}$ .

the NV center to split the energy levels of  $m_s = \pm 1$ . The two electronic transition frequencies corresponding to  $m_s = 0 \rightarrow m_s = \pm 1$  are determined to be  $2042\text{MHz}$  and  $3696\text{MHz}$  via an ODMR measurement. The effective two-level system we use is formed by the sublevel  $m_s = -1 \equiv |\uparrow\rangle$  and  $m_s = 0 \equiv |\downarrow\rangle$ . Interaction with  $^{13}\text{C}$  nuclear spin bath is the dominating source of decoherence for ultrapure IIa type crystals which were used in our experiments. This relatively slow bath is ideal for decoupling experiments [21]. Significant progress was achieved in material engineering [33] but not all sources of magnetic noise can be eliminated in this way, in particular for implanted NV defects [31].

In our experiment, we first polarize the NV center electron spin into the sublevel  $m_s = 0$  with a green laser ( $532\text{nm}$ ). We note that this is equivalent to the preparation of an initial coherent superposition for the relative phase  $\varphi \neq n\pi$ , namely  $|m_s = 0\rangle \equiv |\downarrow\rangle \propto \cos \frac{\varphi}{2} |\uparrow\rangle - \sin \frac{\varphi}{2} |\downarrow\rangle$ . For comparison, we start by applying a single driving field on resonance with the electronic transition  $m_s = 0 \leftrightarrow m_s = -1$ . We measure the oscillation of the population of state  $m_s = 0$ . It can be seen from Fig. 2(a) that the Rabi oscillation decays in a few microseconds. By fitting the experimental data with a Gaussian decay envelope  $S_1(\tau) = \exp(-b_1^2 \tau^2 / 2)$  (see SI for details), we estimate that the decay rate of Rabi oscillation is  $b_1 \approx 88\text{kHz}$ . We stress that the fast decay is mainly due to intensity fluctuations of the microwave field, as the Rabi frequency is  $40\text{MHz}$ , which is strong enough to suppress the effect of

magnetic noise almost completely (the nuclear spin bath formed by  $^{13}\text{C}$  nuclei is slow compared to driving frequency). This statement will be supported and verified by the experimental data that we present here.

To demonstrate the working principle of our concatenated continuous dynamical decoupling, we add a second-order driving field with a weaker amplitude than the first driving. The measured population of the sublevel  $m_s = 0$  can be written as (see SI for a derivation)

$$P_0(\tau) = \frac{1}{2} + \frac{1}{2} \cos \varphi \cos(\Omega_1 \tau + \varphi) + \frac{1}{2} \sin \varphi \sin(\Omega_1 \tau + \varphi) \cos\left(\frac{\Omega_2}{2} \tau\right). \quad (6)$$

We remark that it is not necessary to fix the relative phase  $\varphi$  between two driving fields for the estimation of coherence times. The measured signal averaging over random phase  $\varphi$  leads to  $\bar{P}_0(\tau) = \frac{1}{2} + \frac{1}{4} \cos(\Omega_1 \tau) + \frac{1}{4} \cos(\Omega_1 \tau) \cos(\frac{\Omega_2}{2} \tau)$ . The oscillatory components and their decay features remain the same as a fixed phase.

The second term in Eq.(6) represents Rabi oscillations from the first-order driving. Its decay is mainly due to the fluctuation of the first-order driving field, the effect of which now in the interaction picture is causing the relaxation of the dressed qubit and will be suppressed by the energy gap induced by the second-order driving. To demonstrate this, we first show that CCD scheme can sustain Rabi oscillations by applying a second-order driving field, the intensity of which is ten times weaker than the first driving field. In Fig. 2 (b), we observe coherent Rabi oscillation after  $300, 500, 800, 1000\mu\text{s}$ , and find that it decays significantly slower than the one using only a single driving field (see Fig. 2a for comparison). Our experimental data thus demonstrates that the effect of the fluctuation of the first driving field can be significantly suppressed by a second-order driving field.

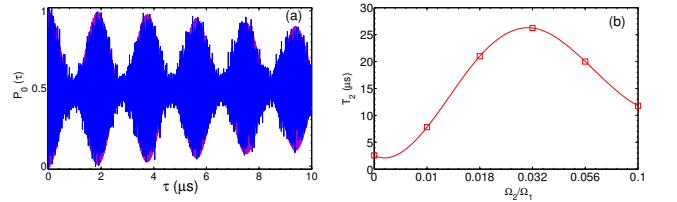


FIG. 3. (Color online) **a**: The measured state population of the sublevel  $m_s = 0$  as a function of the evolution time  $\tau$ . The blue curve is the experimental data, and the purple curve is numerical fitting. The Rabi frequency of the first driving is  $\Omega_1 = 40\text{MHz}$ , and the intensity of the second driving is three orders of magnitude weaker. **b**: The estimated coherence time of the second-order dressed qubit as a function of the amplitude of the second-order driving. The Rabi frequency of the first driving is  $\Omega_1 = 40\text{MHz}$ . We fit the experimental data with a Gaussian decay envelope for the Rabi oscillation and the beatings from the second-order driving respectively.

We further estimate the dephasing time of the second-order dressed qubit by numerically fitting the decay of beatings (i.e. the third term in Eq.(6)), which reflects the coherence of the second-order dressed qubit. The decay stems from the fluctuations of both the first and second driving fields. Our experimental data, in combination with numerical fitting, as plotted in Fig.3 (b), shows that there is an optimal amplitude for the second-order driving field in order to achieve the best coherence time. By increasing the amplitude of the second-order driving one can suppress the effect of the fluctuation in the first driving field, however this will result in larger fluctuations of the second-order driving itself. The compromise between these two effects leads to the optimal choice of a second-order driving. In our experiment, with a second-order driving field about 1000 times less intense than the first-order driving, one can prolong the coherence by an order of magnitude from  $T_2 = 2.5\mu\text{s}$  to  $T_2 \cong 25\mu\text{s}$ , see Fig.3 (a-b). Such a weak additional driving would not have apparent effect in suppressing environmental magnetic noise, nevertheless it significantly improves the dynamical decoupling efficiency. This fact supports our claim that the fast decay of Rabi oscillation in Fig.2(a) is mainly due to the fluctuation in the driving field, which is shown to be a severe problem in conventional continuous dynamical decoupling with a single drive.

We also demonstrate another important ingredient for concatenated continuous dynamical decoupling, namely fixing the relative phase between consecutive driving fields, in order to generate a long living dressed qubit. We achieved this goal by using arbitrary waveform generator (AWG) to generate the first- and second-order driving fields. In Fig.4, we show an example measurement with an estimated fixed phase  $\varphi = 2\pi/5$ .

*Potential applications of CCD.*— The CCD scheme can be combined with various quantum information process-

ing tasks and make them robust against not only noise but also the fluctuations of decoupling fields. The initialization, coherent manipulation and readout for the second-order dressed qubit can be easily achieved with a continuous driving field at the frequency  $\omega_c = \omega + \Omega_2/2$  and with the same phase as the first-order driving. Such a qubit encoded with the sequential dressed states has an ultralong coherence time, and thereby can be exploited to construct a single-spin magnetometer to probe a weak oscillating magnetic field  $b(t) = b_{AC} \cos[(\Omega_1 + \Omega_2/2)t]$ . If  $b_{AC}$  is much larger than the fluctuation of the second driving field, the sensitivity will be  $\sim 1/\sqrt{T_1}$  with  $T_1$  the coherence time demonstrated in Fig.2(a); otherwise it scales as  $1/\sqrt{T_2}$  with  $T_2$  the prolonged dephasing time. The scheme can also be beneficial for the construction of a precise noise spectrometer [26, 35]. We note that the inhomogeneity over an ensemble of quantum systems (namely spatial fluctuation) also leads to dephasing of the ensemble collective state. Our schemes can suppress this kind of spatial fluctuation and in the mean time can be robust against the inhomogeneity of the driving field itself, which may be useful in the ensemble-based magnetometer and quantum memory [36].

*Summary.*— We have introduced the concept of CCD and implemented it experimentally. Using an NV center in diamond we demonstrated the superior performance of concatenated continuous dynamical decoupling compared to single driving fields in extending coherence times of a dressed qubit. A qubit encoded in the concatenated dressed states is robust against both environmental dephasing noise and intensity fluctuation of driving fields. Our schemes can be applied to a wide variety of quantum systems where they may find applications in the construction of nano-scale magnetometry and imaging e.g. with the NV center in diamond, and in the construction of fault-tolerant quantum gates that are protected against noise and control errors.

*Acknowledgements* The work was supported by the Alexander von Humboldt Foundation, the EU Integrating Project Q-ESSENCE, the EU STREP PICC and DIAMANT, the BMBF Verbundprojekt QuOReP, DFG (FOR 1482, FOR 1493, SFB/TR 21) and DARPA. J.-M.C was supported also by a Marie-Curie Intra-European Fellowship within the 7th European Community Framework Program.

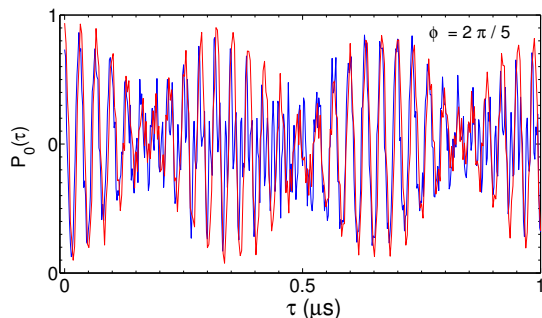


FIG. 4. (Color online) The measured state population of the sublevel  $m_s = 0$  as a function of the evolution time  $\tau$ . The blue curve is the experimental data, and the red curve is from numerical simulation with the estimated relative phase  $\varphi = 2\pi/5$ . The Rabi frequency of the first driving is  $\Omega_1 = 30\text{MHz}$ , and the second driving is  $\Omega_2 = \Omega_1/10$ .

- [1] J. R. Maze, *et. al.*, Nature **455**, 644 (2008).
- [2] G. Balasubramanian, *et. al.*, Nature **455**, 648 (2008).
- [3] G. de Lange, D. Riste, V. V. Dobrovitski, and R. Hanson, Phys. Rev. Lett. **106**, 080802 (2011).
- [4] J. A. Jones et al., Science **324**, 1166 (2009).
- [5] E. L. Hahn, Phys. Rev. **80**, 580594 (1950).
- [6] L. Viola and S. Lloyd, Phys. Rev. A **58**, 2733 (1998).
- [7] P. Facchi, D. A. Lidar, and S. Pascazio, Phys. Rev. A **69**,

- 032314 (2004).
- [8] F. F. Fanchini, J. E. M. Hornos, and R. d. J. Napolitano, Phys. Rev. A **75**, 022329 (2007)
- [9] K. Khodjasteh and D. A. Lidar, Phys. Rev. Lett. **95**, 180501 (2005).
- [10] G. S. Uhrig, Phys. Rev. Lett. **98**, 100504 (2007).
- [11] P. Rabl, P. Cappellaro, M. V. Gurudev Dutt, L. Jiang, J. R. Maze, and M. D. Lukin, Phys. Rev. B. **79**, 041302 (2009).
- [12] A. Bermudez, F. Jelezko, M. B. Plenio, A. Retzker, Phys. Rev. Lett. **107**, 150503 (2011).
- [13] A. Bermudez, P. O. Schmidt, M. B. Plenio, A. Retzker, Phys. Rev. A **85**, 040302(R) (2012).
- [14] N. Timoney, I. Baumgart, M. Johanning, A. F. Varon, M. B. Plenio, A. Retzker, Ch. Wunderlich, Nature **476**, 185-188 (2011).
- [15] M. J. Biercuk, H. Uys, A. P. VanDevender, N. Shiga, W. M. Itano and J. J. Bollinger, Nature **458**, 996-1000 (2009).
- [16] J. Du, X. Rong, N. Zhao, Y. Wang, J. Yang and R. B. Liu, Nature **461**, 1265-1268 (2009).
- [17] G. de Lange, Z. H. Wang, D. Riste, V. V. Dobrovitski, R. Hanson, Science **330**, 60 (2010).
- [18] C. A. Ryan, J. S. Hodges, and D. G. Cory, Phys. Rev. Lett. **105**, 200402 (2010).
- [19] A. M. Souza, G. A. Alvarez, and D. Suter, Phys. Rev. Lett. **106**, 240501 (2011).
- [20] S. Damodarakurup, M. Lucamarini, G. Di Giuseppe, D. Vitali, and P. Tombesi, Phys. Rev. Lett. **103**, 040502 (2009).
- [21] B. Naydenov, F. Dolde, Liam T. Hall, C. Shin, H. Fedder, L. C.L. Hollenberg, F. Jelezko, J. Wrachtrup Phys. Rev. B **83**, 081201(R) (2011).
- [22] A. Laraoui and C. A. Meriles, Phys. Rev. B **84**, 161403(R) (2011).
- [23] T. van der Sar *et. al.*, Nature **484**, 82 (2012).
- [24] G. D. Fuchs, G. Burkard, P. V. Klimov and D. D. Awschalom, Nature Physics **7**, 789-793 (2011).
- [25] H. Fedder, F. Dolde, F. Rempp, T. Wolf, P. Hemmer, F. Jelezko, J. Wrachtrup, Applied Physics B: Lasers and Optics **102**, 497-502 (2010).
- [26] J.-M. Cai, F. Jelezko, M. B. Plenio, A. Retzker, arXiv: 1112.5502.
- [27] R. Hanson, V. V. Dobrovitski, A. E. Feiguin, O. Gywat, Science **320**, 352 (2008).
- [28] L. Childress, M. V. Gurudev Dutt, J. M. Taylor, A. S. Zibrov, F. Jelezko, J. Wrachtrup, P. R. Hemmer and M. D. Lukin, Science **314**, 281 (2006).
- [29] F. Jelezko, T. Gaebel, I. Popa, M. Domhan, A. Gruber, and J. Wrachtrup, Phys. Rev. Lett. **93**, 130501 (2004).
- [30] L. Jiang, J. S. Hodges, J. Maze, P. Maurer, J. M. Taylor, A. S. Zibrov, P. R. Hemmer, and M. D. Lukin, Science **326**, 267 (2009).
- [31] P. Neumann *et al.*, Nature Physics **6**, 249 (2010).
- [32] J. Wrachtrup and F. Jelezko, J. Phys.: Condens. Matter **18**, S807-824 (2006).
- [33] G. Balasubramanian, *et. al.*, Nature Materials **8**, 383 - 387 (2009).
- [34] J. M. Taylor, P. Cappellaro, L. Childress, L. Jiang, D. Budker, P. R. Hemmer, A. Yacoby, R. Walsworth and M. D. Lukin, Nature Physics **4**, 810 (2008).
- [35] T. Yuge, S. Sasaki, and Y. Hirayama, Phys. Rev. Lett. **107**, 170504 (2011).
- [36] J.-M. Cai *et. al.*, work in preparation.

## SUPPLEMENTARY MATERIAL

*Derivation of a second-order dressed qubit.*— In our concatenated scheme, in general, we can apply n-order continuous driving fields on the condition that two subsequent drivings describe rotations about orthogonal axes in the interaction picture. To illustrate the basic principle, we present the calculation details for the derivation of a second-order qubit. The system Hamiltonian is

$$H_0 = \frac{\hbar\omega}{2} (|\uparrow\rangle\langle\uparrow| - |\downarrow\rangle\langle\downarrow|) \quad (7)$$

We apply two driving fields as

$$H_{d_1} = \hbar\Omega_1 \cos(\omega t)\sigma_x \quad (8)$$

$$H_{d_2} = \hbar\Omega_2 \cos[(\omega + \Omega_1)t + \varphi]\sigma_x. \quad (9)$$

where  $\sigma_x = |\uparrow\rangle\langle\downarrow| + |\downarrow\rangle\langle\uparrow|$ . In the first-order interaction picture with respect to  $H_0$  and taking account of a rotating wave approximation, the effective Hamiltonian is

$$H_I^{(1)} = \frac{\hbar\Omega_1}{2}\sigma_x + \frac{\hbar\Omega_2}{2} \left[ e^{-i(\Omega_1 t + \varphi)} |\uparrow\rangle\langle\downarrow| + e^{i(\Omega_1 t + \varphi)} |\downarrow\rangle\langle\uparrow| \right]. \quad (10)$$

The first driving field  $H_{d_1}$  describes rotation about the  $\hat{x}$  axis. In the second-order interaction picture with respect to  $H_0^{(0)} = \frac{\hbar\Omega_1}{2}\sigma_x$ , the effective Hamiltonian becomes

$$H_I^{(2)} = \frac{\hbar\Omega_2}{4} (\sin\varphi\sigma_y - \cos\varphi\sigma_z) \quad (11)$$

where  $\sigma_y$  and  $\sigma_z$  are Pauli operators in the spin up and down basis. Thus, one can see that the second driving field, although it is off-resonant with the original transition frequency  $\omega$ , describes rotation along the axis  $\hat{n}(\varphi, -\pi/2)$  that

is orthogonal to  $\hat{x}$ . For each specific value of the relative phase  $\varphi$ , the eigenstates of  $H_I^{(2)}$  as in Eq.(4-5) in the main text can be used a dressed qubit to encode quantum information. In the above derivations, we have adopted the rotating wave approximations which hold when  $\Omega_2/2 \ll \Omega_1 \ll 2\omega$ . These conditions are fulfilled in the present context.

*Rabi oscillation under a second-order continuous driving.*— In our experiment, we initially prepare the NV spin in the state  $|m_s = 0\rangle \equiv |\downarrow\rangle \propto \cos \frac{\varphi}{2} |\uparrow_\varphi\rangle - \sin \frac{\varphi}{2} |\downarrow_\varphi\rangle$ . The state evolution in the second-order interaction picture is

$$\rho_I^{(2)}(\tau) = \begin{pmatrix} \cos^2 \frac{\varphi}{2} f_0(\tau) + \frac{1}{2}[1 - f_0(\tau)] & -\sin^2 \frac{\varphi}{2} \cos^2 \frac{\varphi}{2} \exp(-i\frac{\Omega_2}{2}\tau) f_1(\tau) f_2(\tau) \\ -\sin^2 \frac{\varphi}{2} \cos^2 \frac{\varphi}{2} \exp(i\frac{\Omega_2}{2}\tau) f_1(\tau) f_2(\tau) & \sin^2 \frac{\varphi}{2} f_0(\tau) + \frac{1}{2}[1 - f_0(\tau)] \end{pmatrix} \quad (12)$$

where the density matrix is written in the basis of  $\{|\uparrow_\varphi\rangle, |\downarrow_\varphi\rangle\}$ ,  $f_0(\tau)$  describes the relaxation from both the limited  $T_1$  of NV center itself and the fluctuation of the first driving field,  $f_1(\tau)$  and  $f_2(\tau)$  represent the dephasing from the relaxation and the fluctuation of the second driving field respectively. We remark that the first driving field is strong enough to eliminate the effect of magnetic noise in our experiment. We measure the population of the state  $|m_s = 0\rangle$  at time  $\tau$ , which can be written as

$$P_0(\tau) = \text{Tr} \left[ \left( \exp \left( -i\frac{\Omega_1\tau}{2} \sigma_x \right) \rho_I^{(2)}(\tau) \exp \left( i\frac{\Omega_1\tau}{2} \sigma_x \right) \right) |\downarrow\rangle \langle \downarrow| \right] \quad (13)$$

$$= \frac{1}{2} + \frac{1}{2} \cos \varphi \cos(\Omega_1\tau + \varphi) f_0(\tau) + \frac{1}{2} \sin \varphi \sin(\Omega_1\tau + \varphi) \cos\left(\frac{\Omega_2}{2}\tau\right) f_1(\tau) f_2(\tau). \quad (14)$$

In the above derivation, we have used

$$\exp \left( i\frac{\Omega_1\tau}{2} \sigma_x \right) |\downarrow\rangle = \cos\left(\frac{\Omega_1\tau}{2} + \frac{\varphi}{2}\right) |\uparrow_\varphi\rangle - \sin\left(\frac{\Omega_1\tau}{2} + \frac{\varphi}{2}\right) |\downarrow_\varphi\rangle. \quad (15)$$

One can estimate the decay functions  $f_i(\tau)$  without fixing the relative phase  $\varphi$ . The observable that we measure is thus the average of  $P_0(\tau)$  over  $\varphi$ , which is as follows

$$\bar{P}_0(\tau) = \frac{1}{2} + \frac{1}{4} \cos(\Omega_1\tau) f_0(\tau) + \frac{1}{4} \sin(\Omega_1\tau) \cos\left(\frac{\Omega_2}{2}\tau\right) f_1(\tau) f_2(\tau). \quad (16)$$

The oscillation contrast will be half of the maximum contrast obtained by fixing a certain relative phase. If the second driving field is sufficiently strong, the effect of the first driving field fluctuation is suppressed and the relaxation decay  $f_0(\tau)$  and  $f_1(\tau)$  will mainly originate from the relaxation of the NV center itself. In such a case, even the oscillation of the third term of Eq.(8) may decay fast, we can still observe that the Rabi oscillations sustain for a long time.

*Numerical simulations of persistent Rabi oscillation.*— We numerically simulate the exact dynamics with two driving fields, namely under the following Hamiltonian

$$H = \frac{\hbar\omega}{2} \sigma_z + \hbar [\Omega_1 + \delta_1(t)] \cos(\omega t) \sigma_x + \hbar [\Omega_2 + \delta_2(t)] \cos[(\omega + \Omega_1)t + \varphi] \sigma_x. \quad (17)$$

where  $\sigma_z = (|\uparrow\rangle \langle \uparrow| - |\downarrow\rangle \langle \downarrow|)$ ,  $\delta_1(t)$  and  $\delta_2(t)$  represent the fluctuations of the first and second driving fields respectively.

We model the fluctuations of driving fields  $\delta_i(t)$   $i = 1, 2$  as an Ornstein-Uhlenbeck process with the correlation function  $C_i(t) = \langle \delta_i(0) \delta_i(t) \rangle = b_i^2 \exp(-|t|/\tau_{c_i})$ , where  $b_i$  is the fluctuation amplitude and  $\tau_{c_i}$  is the correlation time of fluctuation. We generate 2000 realizations of an Ornstein-Uhlenbeck process with the exact simulation algorithm [1]. We first numerically simulated the experimental data in Fig.1(a) for the case of Rabi oscillation with one single driving field. The numerical result agrees well with the experimental data and the Gaussian fit of the decay envelope  $S_1(\tau) = \exp(-b_1^2 \tau^2/2)$  (see Fig.2a of the main text). This supports that an Ornstein-Uhlenbeck process serves as a good model for the driving field fluctuation. We estimate that the relative amplitude fluctuation of the driving field is about  $2 \times 10^{-3}$ . We then use these estimated parameters for the numerical simulation of a second-order driving scheme. Fig.2(b) shows Rabi oscillation with a second-order driving field using the same parameters as in Fig.2(b) of the main text. We note that in the numerical simulation we fixed the relative phase, thus the contrast of Rabi oscillation is twice of Fig.2(b). Nevertheless, the essential feature of the results from our numerical simulation, namely the slow decay of Rabi oscillation, agrees well with the experimental data.



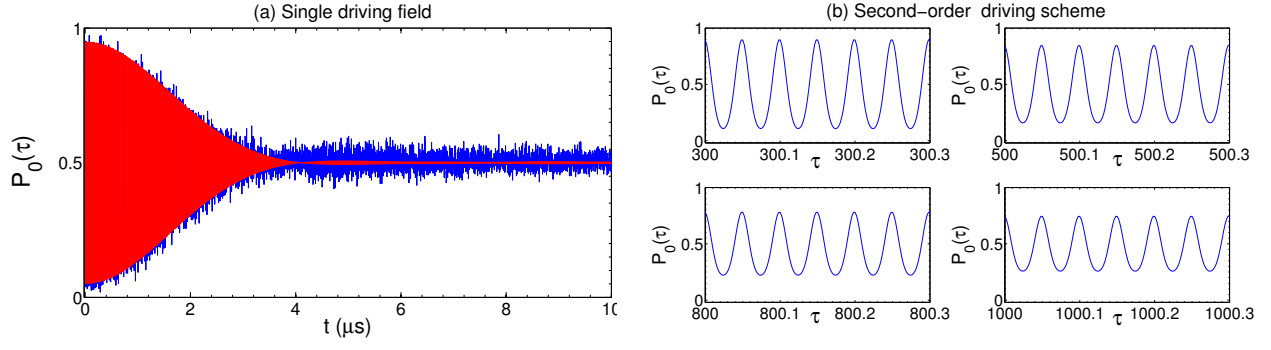


FIG. 5. (Color online) **a**: Numerical simulation of coherent driven oscillation of NV center with a single microwave field (red curve). The blue curve is the experimental data. The Rabi frequency is  $\Omega_1 = 40\text{MHz}$ , and its relative amplitude fluctuation is estimated to be  $\delta_1/\Omega_1 \approx 2 \times 10^{-3}$ . **b**: Numerical simulation of persistent Rabi oscillation by adding a second-order driving field, the intensity of which is 10 times weaker than the first driving ( $\Omega_1 = 20\text{MHz}$ ). The plot shows that Rabi oscillation can sustain for much longer time than one single driving field. The four panels show the very slow decay of the Rabi oscillation beyond  $300\mu\text{s}$ . The decay is mainly due to the relaxation of NV center itself, we use the value of the relaxation time  $T_1 = 1.5\text{ms}$  in the numerical simulations. The relative phase is fixed as  $\varphi = 0$ .

*Coherent manipulation of a dressed qubit in sequential CCD scheme.*— Dressed qubits can be coherently manipulated and coupled with each other via electron spin dipole interaction. To demonstrate this, we take  $\varphi = 0$  as an example. One can apply a continuous field with the frequency  $\omega_c = \omega + \Omega_2/2$  as

$$H_c = g \cos(\omega_c t) \sigma_x \quad (18)$$

In the first-order interaction picture with respect to the original Hamiltonian  $H_0 = \frac{\hbar\omega}{2} (|\uparrow\rangle\langle\uparrow| - |\downarrow\rangle\langle\downarrow|)$ , the coupling can be written as

$$H_c^{(1)} = \frac{g}{2} \left[ \exp(-i\frac{\Omega_2}{2}t) |\uparrow\rangle\langle\downarrow| + \exp(-i\frac{\Omega_2}{2}t) |\downarrow\rangle\langle\uparrow| \right]. \quad (19)$$

In the second-order interaction picture with respect to  $H_0^{(0)} = \frac{\hbar\Omega_1}{2} \sigma_x$ , it becomes

$$H_c^{(2)} = \frac{g}{2} \cos\left(\frac{\Omega_2}{2}t\right) \sigma_x \quad (20)$$

which induces Rabi oscillation between the second-order dressed states.

The dressed qubits can be coupled via dipole-dipole interaction, e.g. between NV electron spins, as follows

$$H_{d-d} = J(3S_z^1 S_z^2 - \vec{S}_1 \cdot \vec{S}_2). \quad (21)$$

In the first-order interaction picture, the electron-electron interaction in the driven Hamiltonian becomes [2]

$$H_{d-d}^{(1)} = 2JS_z^1 S_z^2, \quad (22)$$

The effective interaction between two second-order dressed qubits from the dipole-dipole interaction can be written as

$$H_{d-d}^{(2)} = \frac{J}{2} (\sigma_y^1 \sigma_y^2 + \sigma_z^1 \sigma_z^2 + \sigma_z^1 + \sigma_z^2) \quad (23)$$

where  $\sigma_y$  and  $\sigma_z$  are Pauli operators in the spin up and down basis. The effective entangling coupling between dressed qubits is thus feasible, and can be exploited to construct two-qubit gates.

[1] Daniel T. Gillespie, Phys. Rev. E **54**, 2084 (1996).

[2] A. Bermudez, F. Jelezko, M. B. Plenio, A. Retzker, Phys. Rev. Lett. **107**, 150503 (2011).